Progress in Additive Manufacturing (2020) 5:27–32
https://doi.org/10.1007/s40964-020-00116-8

FULL RESEARCH ARTICLE

SEBM processing of 42CrMo4

Marie Jurisch[1] · Burghardt Klöden[1] · Alexander Kirchner[1] · Gunnar Walther[1] · Thomas Weißgärber[1]

Received: 10 January 2020 / Accepted: 7 February 2020 / Published online: 28 February 2020

Abstract
Powder bed fusion of difficult-to-weld-steels such as the 42CrMo4 applied in this study is a challenging task. These materials are often susceptible to crack formation. To minimize thermal gradients and residual stresses, laser beam technologies generally require preheating of the substrates. Selective Electron Beam Melting (SEBM), on the other hand, is based on preheating the powder bed and, thus, enables crack-free printing even at greater heights. The present study demonstrates the processing of 42CrMo4 by SEBM. Besides parameter optimization, powder analysis, microstructural characterization as well as mechanical testing were carried out both for the as built and heat-treated conditions. The results indicate that the mechanical properties are comparable to those of conventional manufacturing technologies. Furthermore, a generic demonstrator with complex structures shows the high potential of SEBM for these particularly challenging steels.

Keywords Additive manufacturing · Selective electron beam melting · Martensitic steel · Hardness · Microstructure

1 Introduction

42CrMo4 belongs to the high strength martensitic steels. Due to their well-defined mechanical behaviour and good ductility as well as wear resistance and toughness, these steels have a wide range of applications. For instance, they are used in the automotive sector, as gearing components, drive or camshafts, diesel injection systems or in hydraulic systems for pumps, vessels and pistons [1]. From an economic point of view martensitic tempering steels are less expensive compared to austenitic stainless steels [2].

Heat treatments based on quenching and tempering and sometimes also nitriding are common.

The extraordinary properties, however, are accompanied by a more difficult machinability and weldability. This can be explained by the comparatively high carbon content (0.4 wt%), which has a direct influence on crack susceptibility and wear resistance.

To reduce machining efforts, Additive Manufacturing (AM) is of particular interest, the powder bed fusion (PBF) technologies for fabricating metallic components especially. Nevertheless, the limited material diversity is still an obstacle for the industrial implementation of AM processes like laser or electron beam PBF (L-PBF or E-PBF) in the steel sector.

According to literature, 1.3340 (AISI M2) [3], 1.2344 (H13) [4–7], 1.2343 (H11) [8], FeCrMoVC [9], X110CrMoVAl 8–2 [10], X40CrMoV5-1 [11], X65MoCrWV3-2 [12], CP2M® [13] and Rapidur PM-23® [14] belong to the martensitic steels that are evaluated for PBF. The formation of martensite leads to high residual stresses during laser PBF, which can lead to cracking and distortion of the components [6]. These problems can be reduced by substrate heating [4]. In the case of larger component heights, however, distortions can occur again as a result of the temperature gradients and inhomogeneous microstructures.

Heating the powder bed within each powder layer instead of heating the substrate, like it is done with E-PBF [15], is, therefore, a viable alternative.

E-PBF or Selective Electron Beam Melting (SEBM) is a powder bed based AM technology for the production of complex metallic components based on selectively melting the powder in a layer-wise manner which is similar to L-PBF [15]. The repeated heating steps result in the reduction of thermal stresses by holding the powder bed at elevated temperature up to about 1100 °C. Additionally, the electron beam is capable of high energy densities and build rates (e.g. 55–80 cm^3/h for Ti-6Al-4 V [16]).

✉ Marie Jurisch
marie.jurisch@ifam-dd.fraunhofer.de

[1] Fraunhofer Institute for Manufacturing Technology and Advanced Materials IFAM, Branch Lab Dresden, Winterbergstrasse 28, 01277 Dresden, Germany

Table 1 Powder size distribution of the powder in different states

Number of builds	*D* (10%)	*D* (50%)	*D* (90%)
0 (µm)	70.4	97.1	154.5
11 (µm)	75.2	104.1	164.3

Table 2 Powder flowability parameters of the as-received and processed powder

No. of builds	Hall flow (50 g)	Density (g/cm^3)		
		Apparent	Tapped	Pycnometer
0	14.7	4.51	5.07	7.78
11	14.5	4.54	5.07	7.79

In this paper, the SEBM processing and heat treatment of the alloy 42CrMo4 and subsequent mechanical properties are investigated.

2 Materials and methods

2.1 Powder and process

Gas atomized 42CrMo4 powder with an approximate particle size between 53 and 150 µm was supplied by M4P, Germany.

Flowability was characterized for 50 g of as-received and processed powders by means of a calibrated funnel with 2.54 mm diameter (Hall flowmeter, DIN ISO 4490). The measurement of the particle size distribution was assessed according to ISO 13320 (Table 1).

Apparent and tap densities were measured by the funnel method (DIN ISO 3923 and DIN ISO 3953) according to Table 2. The chemical composition was determined using a Thermo Scientific 6300 DUO ICP-OES and a LECO TCH600 and CS 230 as given in Table 3.

All experiments were carried out on an Arcam A2X machine with an accelerating voltage of 60 kV and a build size of $150\times150\times10$ mm^3.

Cubic samples with an edge length of 10 mm and a nominal layer thickness of 70 µm were built onto a start plate heated to 850 °C at the beginning. Preheating of the substrate and every powder layer was conducted by a defocused electron beam. All experiments were carried out with a cross snake scan strategy where the direction of the electron beam changes layer-wise by 90°. After finishing, the build chamber cooled down slowly (< 10 K/min). Parameter variations included scan speed, beam power and line offset, which is the lateral distance between two lines.

The following range of parameters was examined:

- Line offset between 0.05 and 0.2 mm
- Scan speed between 1000 and 10,000 mm/s
- Beam power between 200 and 1500 W.

To reveal the microstructures and porosity, samples were polished and etched with Nital in planes parallel and perpendicular to build direction. Mechanical testing was performed according to DIN EN ISO 6892-1. For that, cylindrical samples with a height of 60 mm and a diameter of 10 mm were fabricated in build direction, while rectangular samples ($10\times15\times60$ mm^3) were additionally built horizontally. The samples, type B4x20, were completely machined by turning to compensate for the influence of surface roughness. The hardness was measured by the Vickers test using an Innovatest Falcon 500 instrument.

The material 42CrMo4 is generally used in the quenched and tempered (QT) state, in which it is characterised by a combination of high strength and toughness. As a result of the slow furnace cooling after E-PBF, the material is still in the soft annealed state. Subsequent heat treatment is therefore necessary. To meet the fatigue strength requirements of this material used for highly stressed components, it is advisable to apply hot isostatic pressing (HIP) to the latter. This minimizes defects such as residual pores, which have a significant influence on the fatigue strength of the components. A part of the samples was, therefore, heat treated before machining, either by hot isostatic pressing (HIP), quenching and tempering or a combination of both. Accordingly, the samples were hipped at 1145 °C for 3 h or hardened at 860 °C for 0.5 h and subsequently quenched by oil and tempered at 550 °C for 1.5 h.

3 Results and discussion

3.1 Powder analysis

The 42CrMo4 powder was analyzed regarding its composition, flowability and shape before and after several build jobs. While the composition did not reveal any changes and matches with the manufacturer's data, the flowability seemed to be slightly improved (Table 2).

Figure 1 shows the micrographs of the powders before and after processing by SEBM. The nearly spherical particles shape and their smooth surfaces correspond to the good flow ability. Nevertheless, there are some hollow spheres

Table 3 Nominal chemical composition of the powder

Element	O	C	Si	Mn	Cr	Mo	Fe
wt-%	0.02	0.40	0.1	0.9	1.0	0.2	Bal.

and elongated particles, which can influence the build quality, as well as some satellites that still exist in the recycled powders. The etched cross-sections exhibit a microstructural change, which is related to a heat treatment in the course of the increased process temperatures. After 11 build jobs the medium particle size increased ($D_{11\ \mathrm{Jobs}}$ (50%) 104.1 µm), whereas the amount of finer particles was reduced. The comparison of both powder size distributions is given in Table 1 and Fig. 2.

While the impurity levels did not change in case of oxygen and nitrogen, a slight decrease of 50 ppm in carbon was measured.

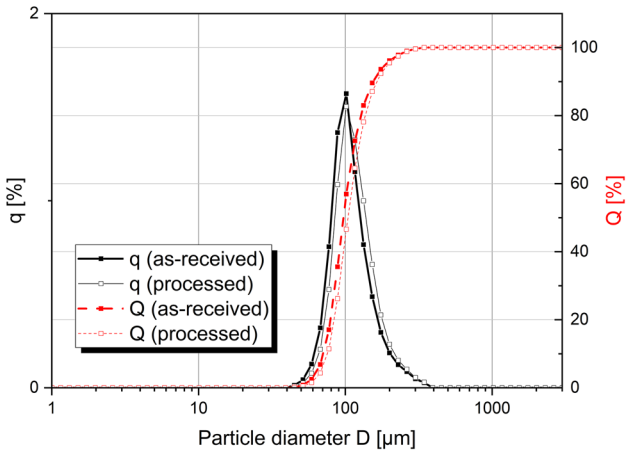

Fig. 2 Powder size distribution of the as-received powder and of the processed powder after 20 build jobs

3.2 Microstructure

The assessment of the process development was determined based on metallographic cross-sections and microstructural characterization.

Depending on the range of process parameters, densities of up to 99.90% could be obtained for energy densities of at least 3 J/mm^2. Figure 3 shows that for beam powers of at least 15 mA the majority of the samples showed crack formation oriented along the grain boundaries of elongated grains in build direction.

In case of 3 J/mm^2 samples with porosities of less than 0.1% without any sign of crack formation could be obtained.

Depending on the cooling rates in the SEBM machine and the hardness achieved, the microstructure (Fig. 4) can be attributed to ferrite (light) and pearlite (dark) in accordance with the time temperature transformation diagram in [1]. Ferrite was built on former austenitic grain boundaries.

Caused by the change in scan length when melting vertically oriented cylindrical samples and due to the faster cooling at the outer positions near the powder bed, the edges revealed finer grains than the center of the specimens which is shown in Fig. 5. Also a slight increase in porosity was detected over the cross-section of the samples. For the specimen in Fig. 5 a porosity of 0.03% in the middle and 0.25% in the fine grained outer ring was measured, respectively.

With the parameter set of Fig. 5 a design demonstrator was built up (Fig. 6). Pre- and post-heating parameters were slightly adapted to account for the variable sample geometry.

The design demonstrator was analyzed by means of 3D measurement. Minimum feature sizes like walls or holes of 0.8 mm with an average deviation of ± 0.4 mm were determined. However, vertical overhangs led to greater distortions, which underlined the need for support structures.

3.3 Mechanical properties

Mechanical properties were analyzed using samples in the as-built as well as heat-treated state. The hardness measurements resulted in a microhardness of 287 ± 5 HV1 (Fig. 7), which is slightly above the hardness in the soft annealed state [1]. This can be attributed to the in situ heat treatment

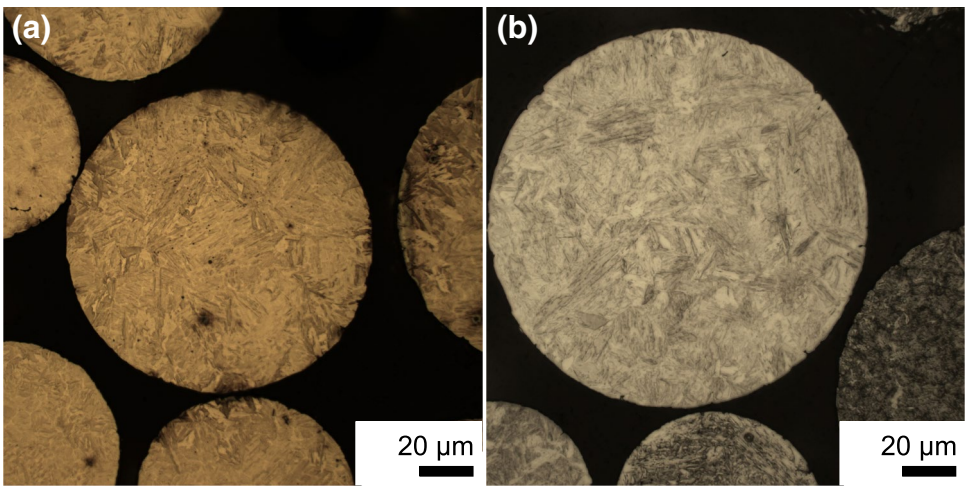

Fig. 1 Microstructure and morphology of **a** as-received and **b** processed powders

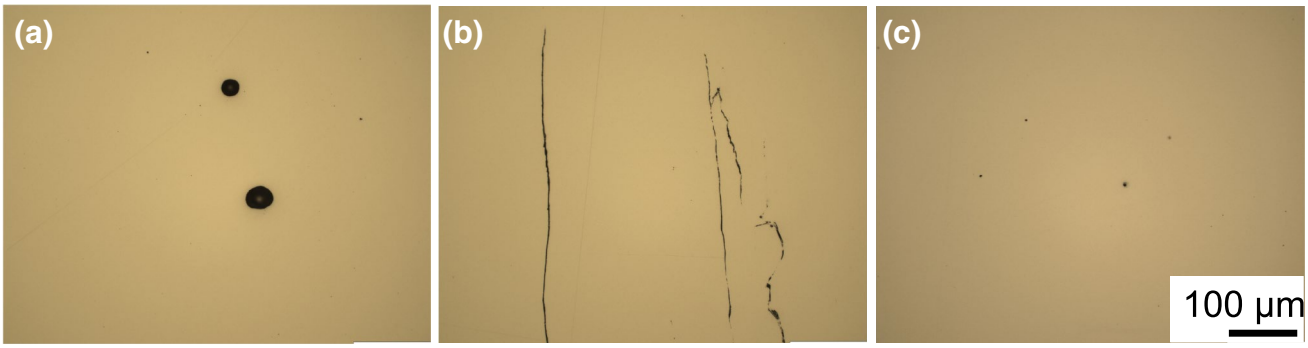

Fig. 3 Optical micrographs of SEBM processed 42CrMo4 powder with the following parameters: **a** 2 J/mm^2, 300 W, **b** 2 J/mm^2, 900 W, **c** 3 J/mm^2, 600 W (build direction is vertical)

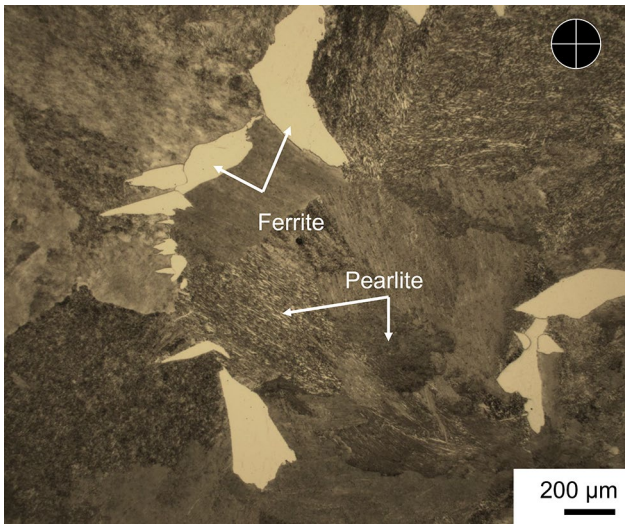

Fig. 4 Microstructure perpendicular to the built direction with ferrite and pearlite phases

at 850 °C during SEBM and conforms to the pearlitic phases from the micrographs (Fig. 4).

The subsequent heat treatment of the specimens was done to raise the hardness up to the target value of 370 HV. A first heat treatment resulted in slightly lower values due to diverging tempering times. A second heat treatment was done to obtain the targeted hardness. Ultimate tensile strength and elongation at break from both treatments compared to the as-built state are given in Figs. 8 and 9, respectively.

The values are in good agreement with the target values according to the data sheet [1]. Even in as-built state the deviations are rather small, which indicates a stable process across the build platform. No further enhancement of tensile strength and a slight increase in elongation from QT- to HIP + QT-state are in agreement with the high initial density of the samples.

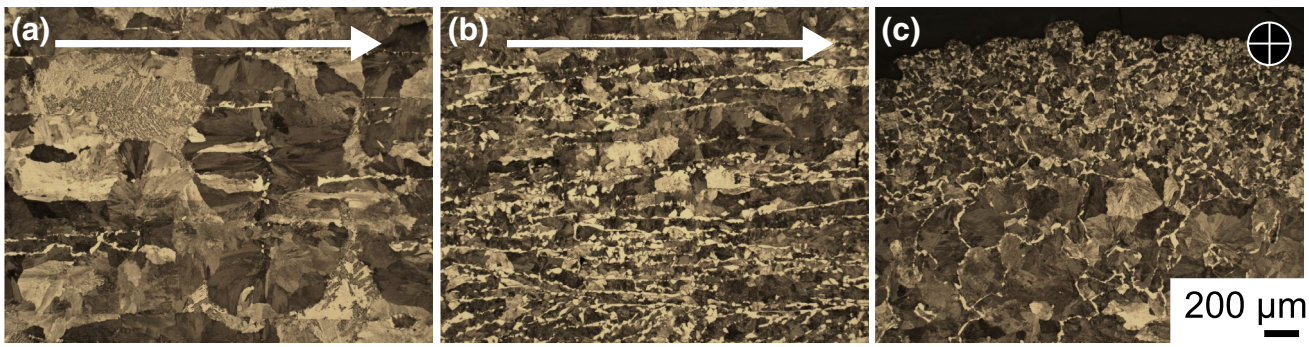

Fig. 5 Micrographs **a** and **b** in and **c** perpendicular to build direction processed with 4000 mm/s and 600 W beam current. Cross-section **a** and **b** were obtained from the middle and edge of the sample, respectively

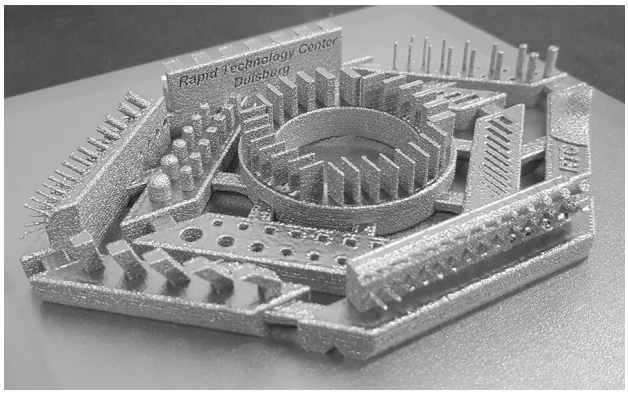

Fig. 6 Design demonstrator to investigate the need of supports with parameters according to Fig. 5

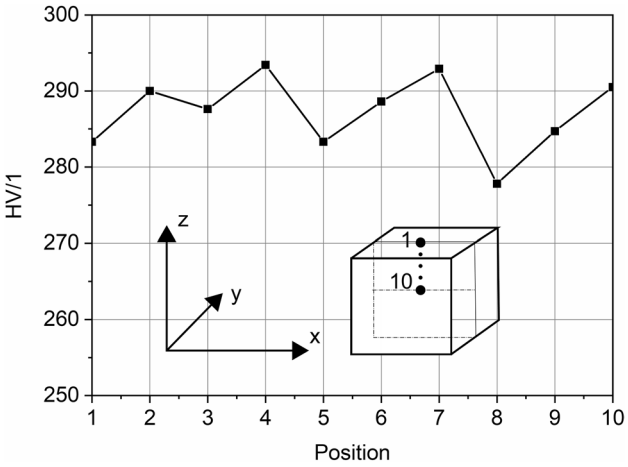

Fig. 7 Measurement of microhardness from top to the middle of a cross-section of a 42CrMo4 sample manufactured according to the parameters used for the sample in Fig. 5

4 Summary and conclusions

Selective Electron Beam Melting of the presented quenching and tempering steel 42CrMo4 was successfully demonstrated for the first time. Therefore, test samples for microstructural analyses as well as a demonstrator were processed.

Due to the susceptibility of this steel to crack formation, maximum beam powers of 600 W and a minimum area energy of 3 J/mm^2 are suggested.

Mechanical properties are comparable to those of conventionally manufactured 42CrMo4.

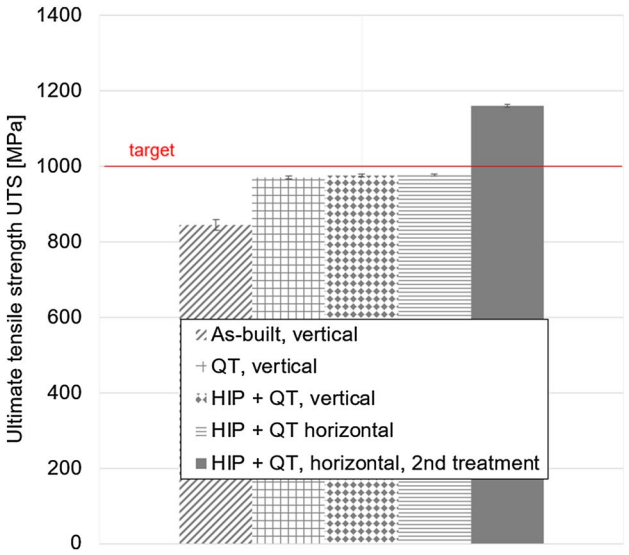

Fig. 8 Ultimate tensile strength in dependence on the sample orientation and heat treatment

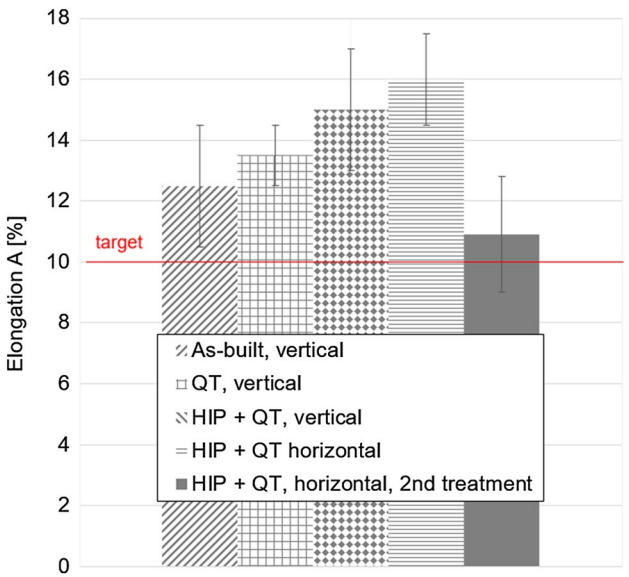

Fig. 9 Ultimate tensile strength in dependence on the sample orientation and heat treatment

Further investigations have to be done in case of differing scan lengths, implementation of support structures and their process parameters. The influence of sample orientation has to be completed additionally by measurement of horizontal specimens.

Acknowledgements Open Access funding provided by Projekt DEAL. The authors gratefully acknowledge the financial support of the Federal Ministry of Education and Research for the research project Agent3D_IMProVe (Grant Number 03ZZ0210B).

Compliance with ethical standards

Conflict of interest The authors declare no conflict of interest.

References

1. Data sheet Firmodur 7225, Deutsche Edelstahlwerke (2015) https://www.dew-stahl.com/fileadmin/files/dew-stahl.com/documents/Publikationen/Werkstoffdatenblaetter/Baustahl/1.7225_1.7227_de.pdf. Accessed 18 Dec 2019
2. Zafra A, Peral LB, Belzunce J, Rodriguez C (2018) Effect of hydrogen on the tensile properties of 42CrMo4 steel quenched and tempered at different temperatures. Int J Hydrog Energy 43:9068–9082. https://doi.org/10.1016/j.ijhydene.2018.03.158
3. Kempen K, Vrancken B, Buls S, Thijs L, Van Humbeeck J, Kruth JP (2014) Selective laser melting of crack-free high density M2 high speed steel parts by baseplate preheating. J Manuf Sci Eng 136:61026-1–61026-6
4. Mertens R, Vrancken B, Holmstock N, Kinds Y, Kruth JP, Van Humbeeck J (2016) Influence of powder bed preheating on microstructure and mechanical properties of H13 tool steel SLM parts. Physics Procedia 83:882–890. https://doi.org/10.1016/j.phpro.2016.08.092
5. Safka J, Ackermann M, Volesky L (2016) Structural properties of H13 tool steel parts produced with use of selective laser melting technology. J Phys Conf Ser. https://doi.org/10.1088/1742-6596/709/1/012004
6. Yan JJ, Zheng DL, Li HX, Jia X, Sun JF, Li YL, Qian M, Yan M (2017) Selective laser melting of H13: microstructure and residual stress. J Mat Sci 52:12476–12485. https://doi.org/10.1007/s10853-017-1380-3
7. Rännar LE, Glad A, Gustafson CG (2007) Efficient cooling with tool inserts. Rapid Prototyp J 13:128–135. https://doi.org/10.1108/13552540710750870
8. Casati R, Coduri M, Lecis N, Andrianopoli C, Vedani M (2017) Microstructure and mechanical behavior of hot-work tool steels processed by selective laser melting. Mater Charact 137:50–57. https://doi.org/10.1016/j.matchar.2018.01.015
9. Sander J, Hufenbach J, Giebeler L, Wendrock H, Kühn U, Eckert J (2016) Microstructure and properties of FeCrMoVC tool steel produced by selective laser melting. Mater Des 89:335–341. https://doi.org/10.1016/j.matdes.2015.09.148
10. Feuerhahn F, Schulz A, Seefeld T, Vollertsen F (2013) Microstructure and properties of selective laser melted high hardness tool steel. Lasers Manuf (LiM 2013) 41:843–848. https://doi.org/10.1016/j.phpro.2013.03.157
11. Krell J, Röttger A, Geenen K, Theisen W (2018) General investigations on processing tool steel X40CrMoV5-1 with selective electron laser melting. J Mater Process Technol 255:679–688. https://doi.org/10.1016/j.jmatprotec.2018.01.012
12. Boes J, Röttger A, Escher C, Theisen W (2018) Microstructure and mechanical properties of X65MoCrWV3-2 cold-work tool steel produced by selective laser melting. Addit Manuf 23:170–180. https://doi.org/10.1016/j.addma.2018.08.005
13. Mutke C, Escher C (2019) Challenges and solution approaches for the processing of a cold work tool steel by means of selective laser melting. In: Proceedings of tooling 2019 conference, 12–16 May 2019, Aachen
14. Jurisch M, Süß M, Kirchner A, Kluge P, Klöden B, Weißgärber T, Kieback B (2018) Selective electron beam melting of tool steels—dimensional limitations. In: Proceedings of euro PM2018 conference, 14–18 Oct 2018, Bilbao. ISBN 978-1-899072-50-7
15. Murr LE, Gaytan SM, Ramirez DA, Martinez E, Hernandez J et al (2012) Metal fabrication by additive manufacturing using laser and electron beam melting technologies. J Mater Sci Technol 28:1–14. https://doi.org/10.1016/S1005-0302(12)60016-4
16. Arcam A2 machine description. https://www.arcam.com/wp-content/uploads/Arcam-A2.pdf. Accessed 17 Dec 2019